VERIFICATION OF UTILITY OF FINITE ELEMENT MODEL FOR MICROSCOPIC DAMAGE SIMULATION OF A FIBER-REINFORCED CERAMIC MATRIX COMPOSITE

R. KITAMURA[a*] and K. GODA[b]

[a] *Graduate School of Science and Engineering, Yamaguchi University, Ube, Japan*
[b] *Department of Mechanical Engineering, Yamaguchi University, Ube, Japan*
**s006wc@yamaguchi-u.ac.jp*

Keywords: CMC (Ceramic Matrix Composites), Matrix crack, Interfacial debonding, FEM (Finite Element Method)

Abstract

Ceramic matrix composites (CMC) such as SiC fiber reinforced SiC ceramic matrix composites (SiC/SiC) are improved in toughness through various mechanisms such as fiber bridging, fiber breakage, pullout, interfacial debonding and matrix crack deflection. To analyze the stress distribution of such damages, in this study, a new finite element model is proposed, in which the effect of Coulomb friction at the interface after fiber breaking or matrix cracking followed by the fiber/matrix debonding is taken into account. The accuracy of the model was validated by comparing with the general-purpose finite element analysis software and theoretical matrix crack model. As a result, the stress distributions behaved non-linearly in the interfacial debonding area, and the present model showed a good agreement with the conventional FEM and theoretical model.

1. Introduction

Ceramics are excellent in heat, abrasion and corrosion resistances, but their strength reliability for structural materials is not enough due to their brittle nature. On the other hand, ceramic matrix composites (CMCs) reinforced with ceramic fibers attract attention as a damage tolerating material, because CMCs are improved in toughness through various mechanisms such as fiber bridging, fiber breakage, pullout, interfacial debonding and matrix crack deflection[1]. Thus, the mechanical behavior of CMCs including such damages should deeply be clarified with engineering significance.

In this study, a new finite element model for the damage analysis of this material is proposed, in which the effect of Coulomb friction at the interface after fiber breaking or matrix cracking followed by the fiber/matrix debonding is taken into account. Although a limitation condition is incorporated into the model, the advantage of this model is such that stress and strain distributions can be obtained by merely one calculation without iteration. The accuracy of the present model was validated by comparing with the results of both the general-purpose finite element analysis software and theoretical matrix crack model.

2. Finite element model and method

2.1 Stiffness equation including contact forces

Once a fiber is broken, matrix cracking or interfacial debonding occurs in a CMC material, and then the whole stiffness of the material is reduced, resulting in a non-linear behavior in the stress-strain relation. For the analysis of this phenomenon, a new method of coordinates updating can be incorporated into the previously proposed analysis updating *K* matrix at damage occurrence [1, 2]. In the new method, the solution is calculated as 'incremental' displacement because the boundary conditions of displacement are given onto the updated coordinates from the previous states. In this situation, the principle of virtual work including contact forces is given as an incremental form, as follows:

$$\iiint_V \Delta\sigma_{ij}\delta\Delta\varepsilon_{ij}dV - \left(\iiint_V \Delta\bar{p}_i\delta\Delta u_i dV + \iint_{S_\sigma} \Delta\bar{T}_i\delta\Delta u_i dS\right) - \iint_C \Delta\bar{F}_i\delta\Delta u_i dS = 0 \tag{1}$$

where σ_{ij}, ε_{ij}, $\bar{p}_i$ and u_i are components of stress, strain, body force and displacement in an elastic body, respectively. $\bar{T}_i$ and $\bar{F}_i$ are surface and contact forces, respectively. In addition, Δ means the increment of each quantity. C is a contact surface and S_σ is a mechanical boundary except C. The subscripts i and j represent r and z-direction, and δ represents the amount of variation. By discretizing Eq. (1) and defining the equivalent nodal force on nodes of each element, the stiffness equation including contact force increment $\{\Delta Q\}$ can be derived as shown in Eq. (2)

$$[K]\{\Delta u\} = \{\Delta f\} + \{\Delta Q\} \tag{2}$$

where $[K]$ is the global stiffness matrix derived from the first term of Eq. (1), $\{\Delta u\}$ is the nodal displacement increment, $\{\Delta f\}$ is the load increment deriving from 2nd and 3rd terms of Eq. (1), and $\{\Delta Q\}$ is treated as an unknown variable vector.

2.2. Definition of interfacial contact states and conditions

Interfacial damage in the vicinity of the breaking point (i.e. matrix crack or fiber breakage) of CMC is considered to be formed as follows: First, interfacial debonding occurs from bonding state which is mechanically balanced. Secondly, interfacial slipping occurs. And finally, the interface becomes a mechanically balanced state again through interfacial friction. Accordingly, we assume interfacial contact states as (a) bonding, (b) interfacial shear debonding, (c) interfacial shear debonding with matrix crack, (d) interfacial shear debonding with fiber breakage, and (e) interfacial re-bonding with friction using the multi-node model between the fiber and matrix, under axisymmetric condition. Figure 1 shows the schematic of such states, where nodes 1 & 3 belong to the fiber element, and nodes 2 & 4 belong to the matrix one. Several interfacial contact conditions are given as Eqs. (3)-(7):

(a) Bonding

When the interface is bonded without debonding as in Figure 1(a), the continuities of displacement and the force balances are given as:

$$\begin{aligned} &\Delta u_1 = \Delta u_2 = \Delta u_3 = \Delta u_4,\ \Delta w_1 = \Delta w_2 = \Delta w_3 = \Delta w_4 \\ &\Delta R_1 + \Delta R_2 + \Delta R_3 + \Delta R_4 = 0,\ \Delta R_1' + \Delta R_2' + \Delta R_3' + \Delta R_4' = 0 \end{aligned} \tag{3}$$

Where, Δu and Δw are displacement increments along r and z-directions. ΔR and ΔR' are contact force increments along r and z-directions of nodes 1 to 4.

(b) Interfacial shear debonding

When the interface is debonded, and slipped along z-direction as in Figure 1(b), the continuities of displacement and the force balances are given as:

$$\begin{aligned} &\Delta u_1 = \Delta u_2 = \Delta u_3 = \Delta u_4, \Delta w_1 = \Delta w_3 \ , \Delta w_2 = \Delta w_4 \\ &\Delta R_1' + \Delta R_3' = \mu(\Delta R_1 + \Delta R_3), \Delta R_2' + \Delta R_4' = \mu(\Delta R_2 + \Delta R_4) \\ &(\Delta R_1 + \Delta R_3) + (\Delta R_2 + \Delta R_4) = 0, \ (\Delta R_1' + \Delta R_3') + (\Delta R_2' + \Delta R_4') = 0 \end{aligned} \tag{4}$$

Where, μ is a coefficient of static friction.

(c) Interfacial shear debonding with matrix crack

When the matrix elements are separated by matrix crack and the interface is debonded and slipped along z-direction as in Figure 1(c), the continuities of displacement and the force balances are given as:

$$\begin{aligned} &\Delta u_1 = \Delta u_2 = \Delta u_3 = \Delta u_4, \Delta w_1 = \Delta w_3 \\ &\Delta R_2' = \mu \Delta R_2, \Delta R_4' = \mu \Delta R_4, \Delta R_1 + \Delta R_3 = 0, \Delta R_1' + \Delta R_3' = 0 \\ &(\Delta R_1 + \Delta R_3) + (\Delta R_2 + \Delta R_4) = 0, \ (\Delta R_1' + \Delta R_3') + (\Delta R_2' - \Delta R_4') = 0 \end{aligned} \tag{5}$$

(d) Interfacial shear debonding with fiber breakage

When the fiber elements are separated by fiber breakage and the interface is debonded and slipped along z-direction as in Figure 1(d), the continuities of displacement and the force balances are given as:

$$\begin{aligned} &\Delta u_1 = \Delta u_2 = \Delta u_3 = \Delta u_4, \Delta w_2 = \Delta w_4 \\ &\Delta R_1' = \mu \Delta R_1, \Delta R_3' = \mu \Delta R_3, \Delta R_2 + \Delta R_4 = 0, \Delta R_2' + \Delta R_4' = 0 \\ &(\Delta R_1 + \Delta R_3) + (\Delta R_2 + \Delta R_4) = 0, \ (\Delta R_1' - \Delta R_3') + (\Delta R_2' + \Delta R_4') = 0 \end{aligned} \tag{6}$$

(e) Interfacial re-bonding with friction

Although the quadruple nodes was debonded and sliped along z-direction, these are re-bonded with friction as in Figure 1(e). Then, the continuities of displacement and the force balances are given as:

$$\begin{aligned} &\Delta u_1 = \Delta u_2 = \Delta u_3 = \Delta u_4, \Delta w_2 = (z_2 / z_1)\Delta w_1, \Delta w_3 = (z_3 / z_1)\Delta w_1, \Delta w_4 = (z_4 / z_1)\Delta w_1 \\ &\Delta R_1 + \Delta R_2 + \Delta R_3 + \Delta R_4 = 0, \Delta R_1' + \Delta R_2' + \Delta R_3' + \Delta R_4' = 0 \end{aligned} \tag{7}$$

Where, z_i (i=1…4) is updated z-direction coordinates of nodes 1 to 4.

2.3. Insertion of the interfacial contact conditions into the stiffness equation

By inserting the interfacial contact conditions of Eqs. (3)-(7) into the stiffness equation (Eq. (2)), the interfacial contact stiffness equation is given as:

$$[K_c]\{\Delta u_c\} = \{\Delta f\} \tag{8}$$

Where, $[K_c]$ is the partly changed stiffness matrix by interfacial contact conditions, of which the detail is shown in the reference [1, 2], and $\{\Delta u_c\}$ is the nodal displacement vector contains nodal contact force (e.g. ΔR and ΔR'). From Eq. (8), $\{\Delta u_c\}$ can be calculated by the Gaussian elimination, and the nodal displacement $\{\Delta u\}$ can be obtained by the continuities of displacement as in Eq. (3)-(7).

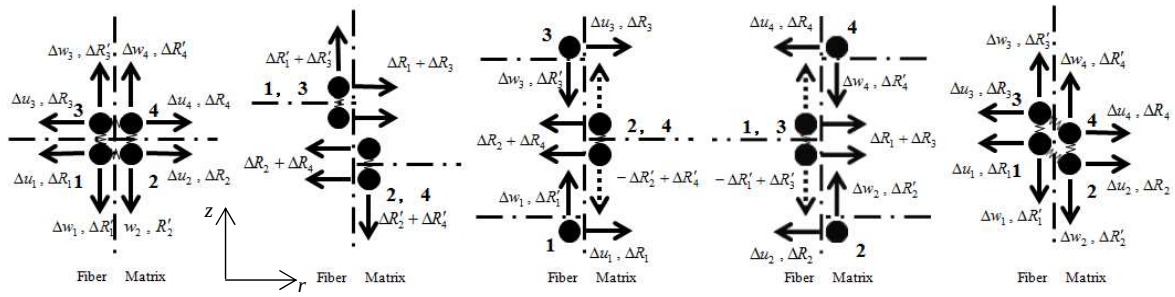

Figure 1. Interfacial contact states (a) Bonding, (b) Interfacial shear debonding, (c) Interfacial shear debonding with matrix crack, (d) Interfacial shear debonding with fiber breakage and (e) Interfacial re-bonding with friction.

2.4. Element and boundary conditions

In many papers [3-7], it is reported that the interfacial debonding of CMC occurs with a quite large scale, and results in relaxation of stress concentration around the matrix cracks or fiber breaks. Accordingly, we assumed that the effects of stress concentration around broken fibers and mutual interference between the fibers are negligible. In this study, we used an axisymmetric model in which a single fiber (r_f=0.0055 mm) is embedded in a cylindrical matrix (r_m=0.011 mm) as shown in Figure 2. And the boundary conditions are given by; 1) z-axis direction fixation at z=0, and 2) load boundary condition $\Delta P=\pi r_m^2 \Delta\sigma$ at the top of the model.

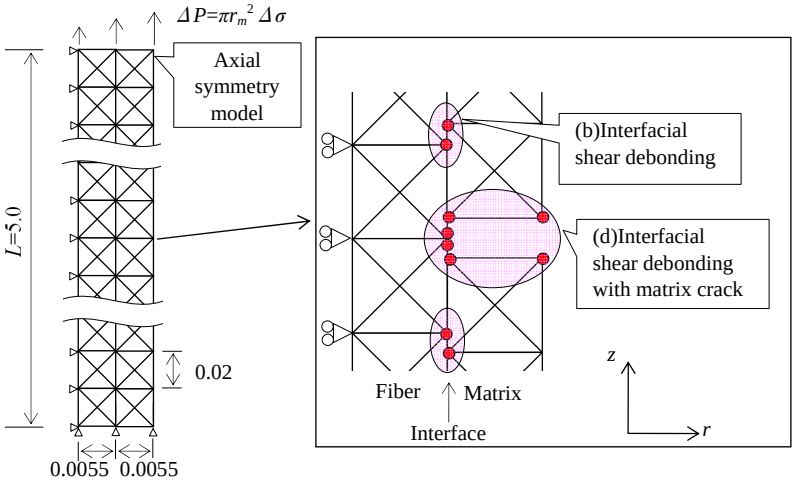

Figure 2. Present finite element model.

3. Theoretical matrix crack model

According to the papers [8-11], temperature change causes thermal strain in CMC, and clamping stress occurs in the interface between the fiber and matrix. Chiang [8] proposed the theoretical matrix crack model considering such thermal strain, in the state that interfacial

debonding L_d occurs around the matrix crack (see, Figure 3). According to the paper, the *z*-axial stresses of the fiber, σ_f and matrix, σ_m, and the interfacial shear stress τ_i in the interfacial debonding ($0 \leqq z \leqq L_d$) region given as:

$$\sigma_f(z) = \frac{\sigma}{V_f} - \frac{\alpha v_f (\sigma - \bar{\sigma})}{V_f(\alpha v_f + \gamma v_m)}\left(1 - e^{-\lambda z}\right) \tag{9}$$

$$\sigma_m(z) = \frac{\alpha v_f (\sigma - \bar{\sigma})}{V_m(\alpha v_f + \gamma v_m)}\left(1 - e^{-\lambda z}\right) \tag{10}$$

$$\tau_i(z) = \frac{r_f \lambda \alpha v_f (\sigma - \bar{\sigma})}{2V_f(\alpha v_f + \gamma v_m)} e^{-\lambda z} \tag{11}$$

On the other hand, the stresses in the interfacial bonding ($z>L_d$) region are given as:

$$\sigma_f(z) = \left[\frac{\sigma}{V_f} - \frac{\alpha v_f (\sigma - \bar{\sigma})}{V_f(\alpha v_f + \gamma v_m)}\left(1 - e^{-\lambda L_d}\right) - \sigma_f(\infty)\right] e^{-\rho(z - L_d)/r_f} + \sigma_f(\infty) \tag{12}$$

$$\sigma_m(z) = \frac{\sigma}{V_m} - \gamma\left\{\left[\frac{\sigma}{V_f} - \frac{\alpha v_f (\sigma - \bar{\sigma})}{V_f(\alpha v_f + \gamma v_m)}\left(1 - e^{-\lambda L_d}\right) - \sigma_f(\infty)\right] e^{-\rho(z - L_d)/r_f} + \sigma_f(\infty)\right\} \tag{13}$$

$$\tau_i(z) = \frac{\rho}{2}\left[\frac{\sigma}{V_f} - \frac{\alpha v_f (\sigma - \bar{\sigma})}{V_f(\alpha v_f + \gamma v_m)}\left(1 - e^{-\lambda L_d}\right) - \sigma_f(\infty)\right] e^{-\rho(z - L_d)/r_f} \tag{14}$$

And, the stresses along the *r*- and θ-axes of the fiber and matrix are given as:

$$(\sigma_r)_f = (\sigma_\theta)_f = \frac{\alpha v_f \sigma_f(z) - v_m \sigma_m(z)}{1 + v_m + 2\gamma + \alpha(1 - v_f)} = q_0(z) \tag{15}$$

$$(\sigma_r)_m = [(r_m / r)^2 - 1]\gamma q_0(z) \tag{16}$$

$$(\sigma_\theta)_m = [-(r_m / r)^2 - 1]\gamma q_0(z) \tag{17}$$

Where,

$$\bar{\sigma} = \frac{V_f q_i}{\alpha v_f}\left[1 + v_m + 2\gamma + \alpha(1 - v_f)\right] \tag{18}$$

$$q_i = \frac{(\alpha_f - \alpha_m) E_m E_f \Delta T}{(1 + v_m) E_f + (1 - v_f) E_m} \tag{19}$$

$$\lambda = \frac{2\mu}{r_f}\kappa = \frac{2\mu}{r_f}\frac{\alpha v_f + \gamma v_m}{1 + v_m + 2\gamma + \alpha(1 - v_f)} \tag{20}$$

$$\sigma_f(\infty) = \frac{1 - 2v_m \kappa}{V_m[\alpha + \gamma - 2\kappa(\alpha v_f + \gamma v_m)]}\sigma \tag{21}$$

$$\sigma_m(\infty) = \frac{1}{V_m}\left[1 - \frac{\gamma(1 - 2v_m \kappa)}{\alpha + \gamma - 2\kappa(\alpha v_f + \gamma v_m)}\right]\sigma \tag{22}$$

$$\rho = \left[\frac{2G_m(\alpha + \gamma - 2\kappa(\alpha v_f + \gamma v_m))}{E_m \ln(\overline{R}/r_f)} \right]^{1/2} \tag{23}$$

$$\ln(\overline{R}/r_f) = -\left[2\ln V_f + V_m(3 - V_f)\right] / \left(4V_m{}^2\right) \tag{24}$$

$$\alpha = E_m / E_f \tag{25}$$

$$\gamma = V_f / V_m \tag{26}$$

where E is a Young's modulus, v is a Poisson's ratio, α is a thermal expansion coefficients, V is a volume fraction, r is a radius and $\sigma(\infty)$ is an axial stress in the bonding region. The subscripts, f and m, represent fiber and matrix, respectively. Furthermore, σ/V_f is the fiber stress at matrix crack surface (z=0), ΔT is temperature change, q_i and $q_0(z)$ are clamping stresses by thermal strain and Poisson's effect, μ is the coefficient of static friction, and $\overline{R}$ ($r_f < \overline{R} < r_m$) is the matrix effective radius (the matrix axial load to be concentrated at $\overline{R}$, and the shear stress carries in the region $r_f \leqq r \leqq \overline{R}$). Chiang [8] said that the clamping stresses are caused by thermal strain and Poisson's effect at the interface between fiber/matrix (i.e. when the thermal expansion $\alpha_f < \alpha_m$, the clamping stress by thermal strain is compression stress; $q_i > 0$), and thus nonlinear stress distributions appear in interfacial debonding region.

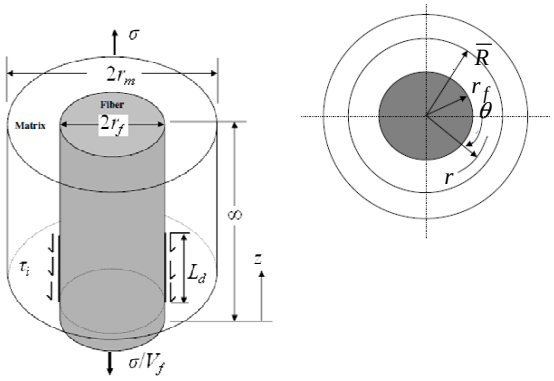

Figure 3. Theoretical matrix crack model [8].

4. Simulation results of the present finite element model and comparison with theoretical model and general-purpose finite element analysis

The results from present finite element model and general-purpose finite element analysis software ANSYS are shown in Figures 4 and 5, and the corresponding theoretical curves obtained from theoretical model are shown in Figure 6. In this simulation, the debonding length is assigned as L_d=1.0 mm, Young's modulus $E_f = E_m$=200 GPa, Poisson's ratio $v_f = v_m$=0.2, coefficient of static friction μ=0.05, and no thermal stress occurs (i.e. ΔT = 0 K and q_i=0 MPa), for convenience.

According to the present finite element model, σ_m recovers gradually from matrix crack surface (z=0), while σ_f shows the peak at z=0 (see, Figure 4(a)). This is because the matrix in the vicinity of the crack surface does not deform so much, so that the fiber has to sustain almost all the load. On the other hand, the matrix can deform approaching to the debonding tip through frictional force, and as a result the matrix stress increases. It should be noted that the stresses are changed suddenly at the interfacial debondig tip ($z=L_d$). In the interfacial bonding region, σ_f and σ_m are both constant, and σ_r, σ_θ are both zero (see, Figure 4(b)). This is attributed to the same elastic constants of the fiber and matrix. In the interfacial debonding region, on the other hand, both σ_r and σ_θ indicate a nonlinear distribution, and σ_r on

the matrix acts as a compression stress along *r*- axis. This is because the fiber and matrix have different strains along *z*-axis, as mentioned above. And it causes a change in Poisson's effect, and leads to strain difference along *r*-axis. As a result, the stress distributions are changed at each position along *r*-axis. It is found in Figure 4(b) that the stresses of the outside matrix elements (r=0.0064) are smaller than inside matrix elements (r=0.0101). In the general-purpose finite element analysis, the results agree approximately with the distributions calculated by the present finite element model (see, Figure 5). A slight difference is attributed to the different analysis algorithm of the interfacial contact problem in the present model and ANSYS. In the theoretical model [8], the stresses indicate a nonlinear distribution (see, Figure 6(a)), and both σ_z of the fiber and matrix are in good agreements with the present finite element model results. On the other hand, σ_r and σ_θ are also relatively good agreements about fiber stress, although slight differences are seen on the matrix stress (see, Figure 6(b)).

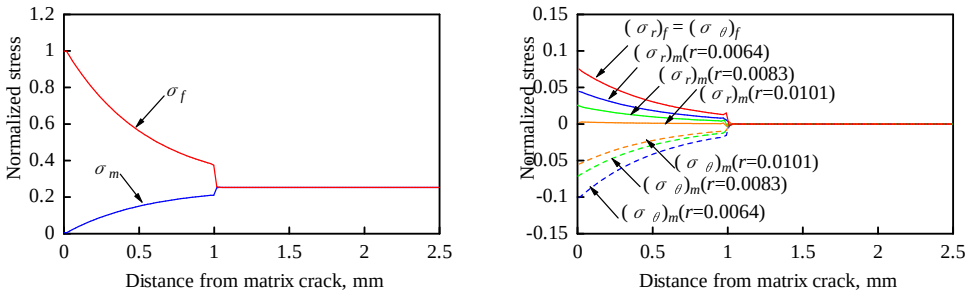

(a) (b)

Figure 4. Stress distribution by present finite element model. (a) along the *z*- axis, (b) along the *r*- and θ- axes.

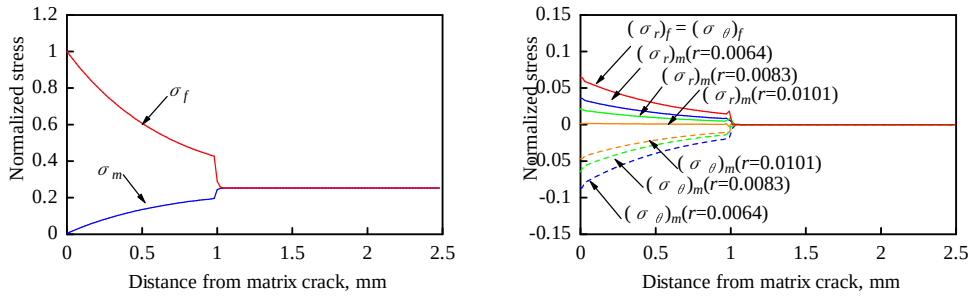

(a) (b)

Figure 5. Stress distribution by general-purpose finite element analysis software ANSYS. (a) along the *z*- axis, (b) along the *r*- and θ- axes

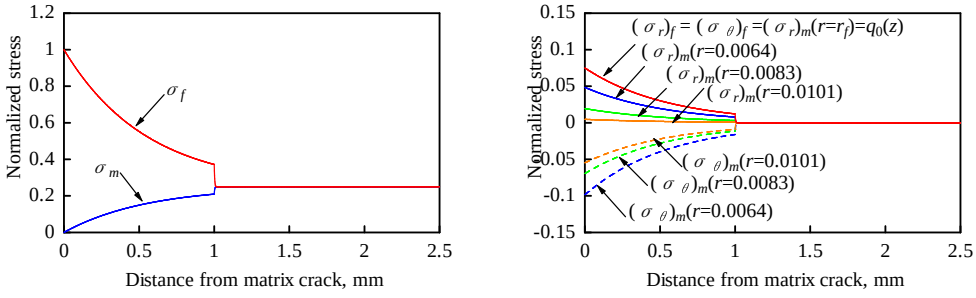

(a) (b)

Figure 6. Stress distribution by theoretical matrix crack model. (a) along the *z*- axis, (b) along the *r*- and θ-axes

5. Conclusion

A new finite element model for the fiber/matrix interfacial debonding and sliding was proposed. The accuracy of this model was validated in comparison with the results of both the general-purpose finite element analysis software ANSYS and theoretical matrix crack model.

The present finite element model results showed that the fiber and matrix stress distributions behaved non-linearly in the interfacial debonding area, while these displayed a constant in the bonding area. And, this model also showed a good compatibility with the general-purpose finite element analysis and theoretical model. Thus, it is expected that this model can be applied for damage states such as not only one matrix crack but also multiple fracture, fiber breakage and matrix crack deflection, indeed difficult through the conventional theoretical models or general-purpose finite element analysis.

References

[1] K. Goda *et al*. FEM Formulation and Strength Simulation by Interfacial Contact Model of Fiber-Reinforced Ceramic Matrix Composites, *Journal of the Japan Society for Composite Materials*, Volme31:184-191, 2005.

[2] R. Kitamura and K. Goda. Verification of damage model of ceramic matrix composites and analysis of cyclic deformation behavior, *Transactions of the Japan Society of Mechanical Engineers*, 2014. (to be published)

[3] H. Cao and M. D. Thouless. Tensile Tests of Ceramic-Matrix Composites: Theory and Experiment, *Journal of the American Ceramic Society*, Volume73:2091–2094, 1990.

[4] W. A. Curtin. Theory of mechanical properties of ceramic-matrix composites, *Journal of the American Ceramic Society*, Volume74:2837- 2845, 1991.

[5] S. L. Phoenix and R. Raj. Scalings in Fracture Probabilities for a Brittle Matrix Fiber Composite, *Acta Metall. Matter*., Volume40:2813-2828, 1992.

[6] Neumeister, J. M. A constitutive law for continuous fiber reinforced brittle matrix composites with fiber fragmentation and stress recovery, *Journal of the Mechanics and Physics of Solids*, Volume41, 1383–1404, 1993

[7] A. Kelly and R. W. Tyson. Tensile properties of fiber reinforced metals, *Journal of the Mechanics and Physics of Solids*, Volume13:329-350, 1965.

[8] Y. C. Chiang. On a matrix cracking model using Coulomb's friction law, *Engineering Fracture Mechanics*, Volume74:1602–1616, 2007.

[9] Li and Y. Song. Estimate interfacial Coefficient of Ceramic Matrix Composites from Hysteresis Loops, *Journal of Composite Materials*, Volume45:989-100, 2010.

[10] J. K. Kim and Y. W. MAI. *Engineered Interfaces in Fiber Reinforced Composites*, ELSEVIER SCIENCE Ltd, Kidlington, 1998.

[11] Gao *et al*.. Fracture of Fiber Reinforced Materials, *Jurnal of Applied Mathematics and Physics*, Volume39:550-572, 1988.